Article

Neuron

Vesicular Release Statistics and Unitary Postsynaptic Current at Single GABAergic Synapses

Highlights

- Variations among single synapses mainly arise from differing docking site numbers
- Docking site number grows with synaptic size
- Docking site occupancy is less than 1 at rest
- Depolarizing prepulses result in reduced docking site occupancy during trains

Authors

Camila Pulido, Federico F. Trigo, Isabel Llano, Alain Marty

Correspondence

alain.marty@parisdescartes.fr

In Brief

The functional role of synaptic docking sites has remained unclear. Pulido et al. demonstrate that variations in docking site number underlies differences among single GABAergic synapses and that docking site occupancy is modulated during synaptic depression and following depolarizing prepulses.

Pulido et al., 2015, Neuron *85*, 159–172
January 7, 2015
http://dx.doi.org/10.1016/j.neuron.2014.12.006

CellPress

Neuron
Article

Vesicular Release Statistics and Unitary Postsynaptic Current at Single GABAergic Synapses

Camila Pulido,[1] Federico F. Trigo,[1] Isabel Llano,[1] and Alain Marty[1,*]
[1]Laboratoire de Physiologie Cérébrale, CNRS UMR 8118, Université Paris Descartes, 45 rue des Saints Pères, 75006 Paris, France
*Correspondence: alain.marty@parisdescartes.fr
http://dx.doi.org/10.1016/j.neuron.2014.12.006

SUMMARY

The existence of vesicular docking sites in central synapses is supported by morphological and biochemical evidence, but their functional role remains elusive. To investigate this role we have studied single depressing GABAergic synapses where multivesicular release and postsynaptic receptor saturation have been documented. We used failure/success patterns to estimate the number of vesicular docking sites, which varied from one to six among synapses. Variations of docking site numbers account for differences in release probability, as well as in the amplitude and decay kinetics of unitary postsynaptic currents. Upon repetitive stimulation, decreasing docking site occupancy likewise accounts for changes both in presynaptic and postsynaptic parameters. Finally steady-state docking site occupancy during train stimulations can be modulated by applying subthreshold presynaptic conditioning potential steps. The results suggest that differences in docking site numbers determine intersynaptic variability and that docking site occupancy is a key parameter controlling single synapse signaling.

INTRODUCTION

Central mammalian synapses differ markedly in terms of quantal size, release probability, and short-term synaptic plasticity. Even within one family of synapses, where both presynaptic and postsynaptic partners belong to single classes of neurons, very heterogeneous synaptic parameters have been reported (review: Branco and Staras, 2009).

Perhaps the most basic of these parameters is size. Individual synapses vary in size on a scale spanning one order of magnitude or more; the surface area of the presynaptic active zone, that of the postsynaptic density, the number of postsynaptic receptors, and the number of synaptic vesicles all increase in parallel with synaptic size (Harris and Stevens, 1988; Schikorski and Stevens, 1997; Nusser et al., 1997). Recently, it was shown that the number of presynaptic calcium channels at individual active zones, as well as the corresponding release probability, increase with active zone size at the calyx of Held (where individual active zones can be investigated with local patch clamping) (Sheng et al., 2012) and at hippocampal glutamatergic synapses (where "optical quantal analysis" can be implemented) (Holderith et al., 2012). Likewise, release probability and synaptic size are correlated in cultured hippocampal neurons (Ermolyuk et al., 2012).

While these studies shed light on variations in vesicular release at single active zones, surprisingly little is known on corresponding variations at the next step of synaptic transmission: postsynaptic current (PSC). Yet the relation between transmitter release and PSCs can be complex, particularly at synapses displaying multivesicular release and/or saturation of postsynaptic receptors. A promising preparation to address these issues is offered by molecular layer interneurons (MLIs) of cerebellar slices, because a sizable fraction of MLI-MLI synapses appears to involve a single synaptic contact, with a single presynaptic active zone and a single postsynaptic density (Nusser et al., 1997; Kondo and Marty, 1998). Like other GABAergic and glycinergic synapses (Biró et al., 2006; Balakrishnan et al., 2009), MLI-MLI synapses display multiple vesicular release events in response to one action potential (AP), but because extensive postsynaptic receptor saturation occurs following vesicular release, the peak PSC amplitude histogram at individual synaptic contacts forms a single Gaussian (Kondo and Marty, 1998; Auger et al., 1998). Previous work showed that quantal size varies markedly among single synapses and that it grows with the size of the postsynaptic density and of the associated number of receptors (Nusser et al., 1997; Auger and Marty, 1997; Kondo and Marty, 1998). Whether other aspects of synaptic transmission, including release probability, the extent of multivesicular release, and short-term synaptic plasticity, also depend on synaptic size remains to be investigated.

A related question concerns possible interactions between multivesicular release and short-term synaptic plasticity in a single synapse. It is widely accepted that synaptic vesicle availability plays a key role in synaptic depression, but it is not known whether the processes of multivesicular release and synaptic depression interact with each other and, if they do, what the functional consequences of such interactions are.

Such issues touch upon elementary mechanisms of the synapse. In recent years, morphological, biochemical, and functional evidence has accumulated supporting the existence in each synaptic contact of several docking sites (sometimes called "release sites"), which are specific macromolecular structures

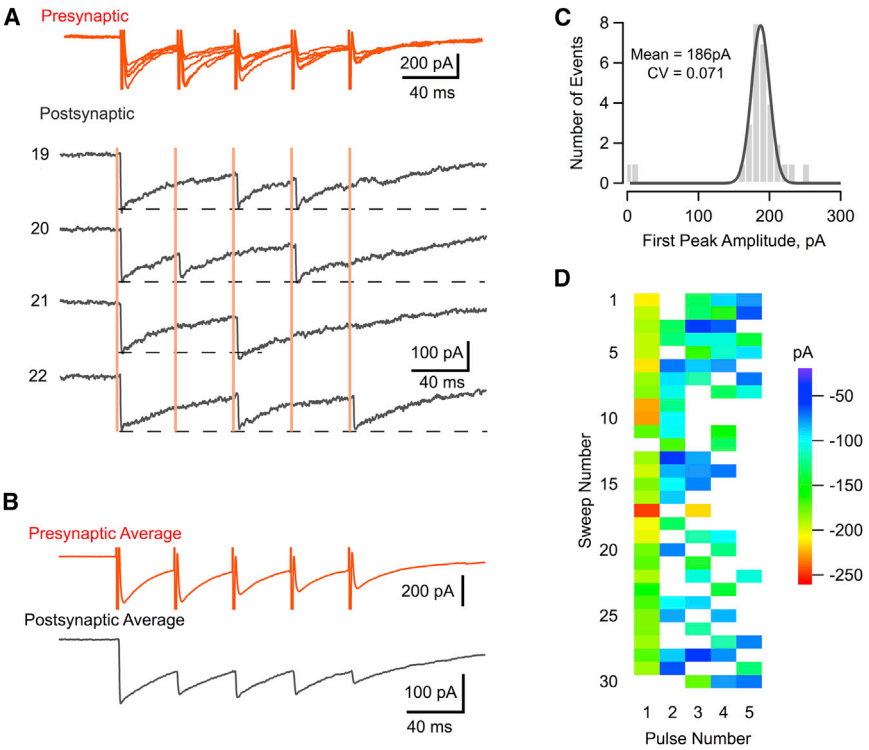

Figure 1. "Simple Synapses" Exhibit Receptor Saturation and Homogeneous PSC Amplitudes

(A) Presynaptic (red superimposed traces, showing autoreceptor currents) and postsynaptic responses (black individual traces; trace numbers correspond to sweep numbers in [D]) to trains of presynaptic APs (five pulses at 25 Hz; timing indicated by vertical pink lines) in a synaptically connected pair of MLIs. PSC peak amplitude increments (measured from the value observed just before each stimulus) are reduced within the train compared to the values for the first stimulus, but the absolute PSC peak values are almost constant within a train (dotted lines), indicating saturation of postsynaptic receptors.

(B) Average presynaptic and PSCs (30 consecutive trials), showing synaptic depression in both cases.

(C) Histogram of first peak PSC amplitudes; single Gaussian fit with low CV are diagnostic of a single synaptic site, called "simple synapse." Success rate: 93%. The position of the histogram peak gives i, the mean amplitude of successful events (= 186 pA).

(D) Pattern of success/response sequences and associated peak PSC amplitudes for a series of 30 consecutive trials. Failures are depicted in white.

where vesicles must bind before undergoing exocytosis (Nagwaney et al., 2009; Szule et al., 2012; reviews: Zucker et al., 2009; Neher, 2010). Variations in docking site occupancy are thought to drive short-term synaptic plasticity (Neher and Sakaba, 2008). However, inferences on the functional role of docking sites mostly originates from multisite synapses. Performing such studies at single synapses, as in the present work, has the potential to provide a more direct test of docking site function.

Recent results using local calcium uncaging indicate that in MLIs, each synaptic contact contains a fixed number of docking sites, which varies from one to four between contacts (Trigo et al., 2012). Here we investigate the influence of the number and occupancy of docking sites on synaptic signals. We first estimate the number of docking sites in individual experiments, based on failure statistics. We then show that variations of docking sites number explain signaling differences between individual synaptic contacts. These differences involve not only release probability and short-term synaptic plasticity but also PSC unitary amplitude and decay kinetics. Moreover, in individual experiments, variations in docking site occupancy during AP trains account for observed changes in failure frequency, peak amplitude, and decay kinetics of PSCs. Altogether the number and occupancy of docking sites emerge as key parameters governing unitary synaptic function.

RESULTS

Simple Synapses Display Decreasing Release Probability during Trains

In the present work, we study failure/success sequences in single synapses following trains of presynaptic APs. PSCs were measured in functionally connected pairs of MLIs from juvenile rats. Each cell was under voltage clamp. The pipette solution contained a high concentration of Cl^- (140 mM) to maximize PSC amplitudes measured at the holding potential (−60 mV). A significant fraction of the synaptic connections between MLIs, called "simple synapses," involve single synaptic contacts (Llano and Gerschenfeld, 1993; Kondo and Marty, 1998). Our first aim was to characterize responses of simple synapses to train stimulations.

A representative recording is shown in Figure 1. Here, 30 trains of five pulses each were given at 25 Hz, with 5 s intervals between trains (ensuring a large degree of recovery between trains: Sakaba, 2008). In response to presynaptic voltage pulses, large autoreceptors/autaptic currents were recorded, reflecting the sensitivity of the presynaptic cell to the neurotransmitter that it releases (Figure 1A, red traces) (Pouzat and Marty, 1998; 1999). On the postsynaptic side, PSCs obtained in response to the first pulse displayed homogeneous amplitudes (Figure 1A, black traces), and the corresponding amplitude histogram could be fitted with a single Gaussian with a small CV (0.071; Figure 1C), indicating a simple synapse. The mean peak amplitude, called simple synapse current hereafter (symbol: i), has a value of 186 pA, in accordance with the large quantal sizes observed at MLI synapses (Llano and Gerschenfeld, 1993; Nusser et al., 1997; Auger et al., 1998). When two PSCs overlapped within a train, the second PSC had a smaller incremental amplitude than the first (Figures 1A and 1D), yet the absolute peak PSC amplitude remained approximately constant (dashed lines in Figure 1A), indicating saturation of postsynaptic receptors (Auger and Marty, 1997; Auger et al., 1998). Mean responses, both presynaptic and postsynaptic, displayed synaptic depression within

a train (Figure 1B). This reflected not only receptor saturation but also a decrease in release probability. Thus, in the example shown (Figure 1D), the probability of success was 93% for the first pulse, 63% for the second, and an average of 51% for the third to fifth pulses.

To investigate possible mechanisms underlying synaptic fluctuations, we first compared peak amplitudes of autoreceptor/autaptic currents and of PSCs across trials, finding no correlation (Figure S1 available online). Because the two sorts of signals are elicited by the same presynaptic AP, these results indicate that trial-to-trial changes in the AP waveform and associated calcium entry do not influence PSC fluctuations significantly.

At the juvenile calyx of Held, Ca^{2+}/calmodulin-dependent inactivation of presynaptic calcium channels elicits a significant decrease in release probability during repetitive stimulation (Xu and Wu, 2005). To examine whether a similar effect occurs in MLIs, we introduced the calcium-sensitive dye Oregon green 488 BAPTA-6F (100–200 μM) in the pipette solution, and we used two-photon imaging in single varicosities to analyze calcium concentration changes following one or two axonal APs (40 ms intervals, corresponding to the interspike interval used in the majority of the present experiments). The calcium responses to the first and second AP were identical (mean amplitude ratio: 0.99 ± 0.06, n = 6; Figure S2). This indicates that synaptic depression occurs downstream of calcium entry.

"Temperature plots" of PSC amplitudes as a function of pulse number and sweep number (Figure 1D) give a visual characterization of functional properties of a simple synapse. As we shall now document, these properties varied markedly across experiments, and the differences followed certain patterns that give clues on the nature of underlying mechanisms.

Heterogeneity among Simple Synapses

A serial electron microscopy section study has shown that most MLI-MLI varicosities involve a single synaptic contact, that synaptic contacts vary markedly in size and in number of postsynaptic receptors, and that the number of postsynaptic receptors varies in register with synaptic size (Nusser et al., 1997). Variations between postsynaptic receptors numbers underlie the marked quantal size heterogeneity observed between simple synapses (Auger and Marty, 1997; Nusser et al., 1997). In our simple synapse recordings, i values varied across experiments from 36 to 221 pA, with a mean of 100 pA; these values are similar to those previously reported (Kondo and Marty, 1998). We next searched for correlations between i, taken as indicator of synaptic size, and other functional parameters of simple synapses.

While Figure 1 illustrates a case where a large value of i is combined with high success probability (defined as the probability to release at least one vesicle), Figure 2 exemplifies an experiment with low i (i = 61 pA in Figure 2C versus 186 pA in Figure 1C) and moderate success probability (54% for the first pulse responses in Figure 2D versus 93% in Figure 1). Strikingly, in spite of the relatively low success rate, the paired pulse ratio (PPR) is lower in the case of Figure 2 (with a value of 0.25; Figures 2B and 2D) compared to that of Figure 1 (with a value of 0.68; Figures 1B and 1D). Also, it may be noted that the half time of PSC decay, $t_{1/2}$, is smaller for the experiment of Figure 2 than for that of Figure 1 ($t_{1/2}$ = 9.9 ms and 39.5 ms respectively).

Group results show a gradual dependence of the success probability in response to the first pulse, $P(S_1)$, as a function of i (Figure 2E; $r = 0.63$; $p < 0.0001$). The regression line indicates a change from a success rate of ~0.4 for the smallest synapses, with i values near 50 pA, to almost 1 for the largest ones, with i values near 200 pA. These results are in line with recent work in glutamatergic synapses suggesting a link between synaptic size and release probability (Ermolyuk et al., 2012; Holderith et al., 2012; Sheng et al., 2012).

It has been suggested that this scaling of the release probability with size results from a larger number of voltage-dependent calcium channels contributing to exocytosis in larger synapses, leading to an enhancement of spike-evoked calcium transients at the site of exocytosis (Holderith et al., 2012; Sheng et al., 2012). Here, volume-averaged peak AP-induced calcium transients did not increase with the size of presynaptic varicosities (Figure S3). In addition, the evolution of success probability during trains was not consistent with an increase of local spike-evoked calcium transients with synaptic size. If this were the case, the amount of synaptic depression would be expected to decrease with synaptic size, as found before (Sheng et al., 2012). In the present case, however, the ratio between the success rate calculated for the last three pulses, $P(S_{3-5})$, to the success rate obtained for the first pulse, $P(S_1)$, failed to decrease with i (Figure 2F). (This ratio varies in parallel to the standard PPR calculated as the ratio $P(S_2)/P(S_1)$, and it is preferred here to the PPR because it is calculated from a larger number of trials, and it is therefore statistically more robust.) These data are not consistent with the proposal that local calcium signals increase with synaptic size.

We therefore considered alternative mechanisms to explain the links between simple synapse current amplitude, release probability, synaptic depression, and PSC decay kinetics. Based on calcium photolysis experiments, it has been suggested that simple synapses contain variable numbers of docking sites and that larger synapses have a more numerous complement of docking sites than smaller ones (Trigo et al., 2012) (Figure 2G). If this is the case, release statistics of large synapses may differ from those of small synapses because they have a larger number of docking sites, rather than a larger number of calcium channels driving exocytosis. Below we explore this possibility.

Modeling Synapse Heterogeneity with Varying Numbers of Docking Sites

Release statistics for a simple synapse containing N equivalent docking sites are described in Experimental Procedures. Each docking site undergoes a cycle starting from an occupied state, followed by exocytosis and docking of a new synaptic vesicle. We call p the probability of an occupied docking site to undergo exocytosis and R the rate constant of recovery to the docked state after exocytosis. Both p and R are assumed constant within a train. Each docking site has a probability δ of being occupied by a release-ready vesicle at rest, so that the average size of the readily releasable pool (RRP) is $n = N\,\delta$. Making $j = 1$ in Equation 5 below gives

$$P(S_1) = 1 - (1 - \delta p)^N. \quad (1)$$

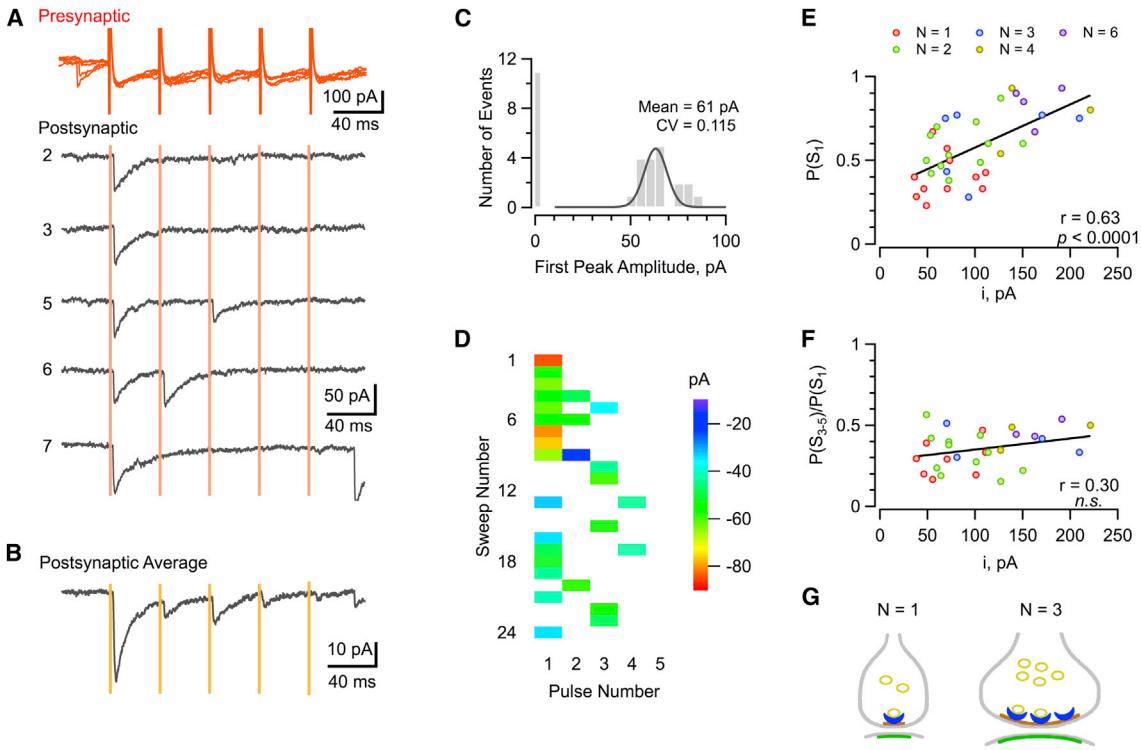

Figure 2. Functional Variability among Simple Synapses

(A) Sample responses (red: presynaptic; black: postsynaptic; trace numbers correspond to sweep numbers in [D]) to AP trains in a presumed single docking site synapse, called "elementary synapse." Note lower PSC amplitude and lower release probability compared to the example of Figure 1, where the number of docking sites was estimated as 6.

(B) Average PSCs from the same experiment showing very pronounced synaptic depression (PPR = 0.25) in spite of the moderate release probability (P(S1) = 0.67).

(C) Histogram of first peak PSC amplitudes (i = 61 pA).

(D) Pattern of success/response sequences and associated peak PSC amplitudes for a series of 24 consecutive trials.

(E) Summary results from 33 simple synapses showing a positive correlation between i and the corresponding probability of success, $P(S_1)$. This indicates a link between the size of simple synapses and the probability of success.

(F) $P(S_{3–5})/P(S_1)$ as a function of i, where $P(S_{3–5})$ represents the success rate measured for stimuli 3–5, fails to show a negative correlation. This argues against release statistics being governed by a scaling of release probability with synaptic size.

(G) Schematic model of a small and of a large simple synapse (active zone in brown and postsynaptic density in green), with respective values of 1 and 3 for N, the number of docking sites (in blue). In (E) and (F), each dot is colored according to the value of N (calculated as explained in Experimental Procedures) that is assigned to the corresponding experiment.

This is an increasing function of N, in agreement with Figure 2E, provided that δ and p are constant. This reflects the fact that $P(S_1)$ includes the contributions of each docking site, and hence increases with N.

In response to the second pulse, the probability of success is as follows:

$$P(S_2) = 1 - (1 - \delta_2 p)^N, \quad (2)$$

where δ_2 is the docking site occupancy just before the second stimulation. δ_2 is smaller than δ for a depressing synapse (Experimental Procedures), and in these conditions it may be shown that the ratio PPR = $P(S_2)/P(S_1)$ is an increasing function of N. Indeed, depression is maximally strong for N = 1, because once the single docking site is empty, no other site can replace it. With increasing N values, there is an increasing likelihood that other docking sites may be filled before the second pulse, and therefore the PPR increases. Overall, the model predicts that both $P(S_1)$ and the PPR grow as a function of N.

As shown in Experimental Procedures (Equation 11), N can be calculated by using an approximate relation derived for the RRP size (n) under the assumption of no recovery (R = 0): $n = log(1 - P(S_1))/log(log(1 - P(S_2))/log(1 - P(S_1)))$.

Having calculated n from this equation, N can be obtained using the relation N = n/δ. As a first approximation, we assumed that δ was 0.7, based on previous calcium photolysis data (Trigo et al., 2012), and N was taken as the integer closest to the value n/0.7. Values of N obtained with this method ranged from 1 to 4 (i.e., in the same range that was previously obtained with calcium photolysis experiments) (Trigo et al., 2012). These provisional N estimates were then revised as explained in Experimental Procedures. The final assignments, with a range going from 1 to 6, are illustrated by color coding in Figures 2E and 2F. Figures 1 and

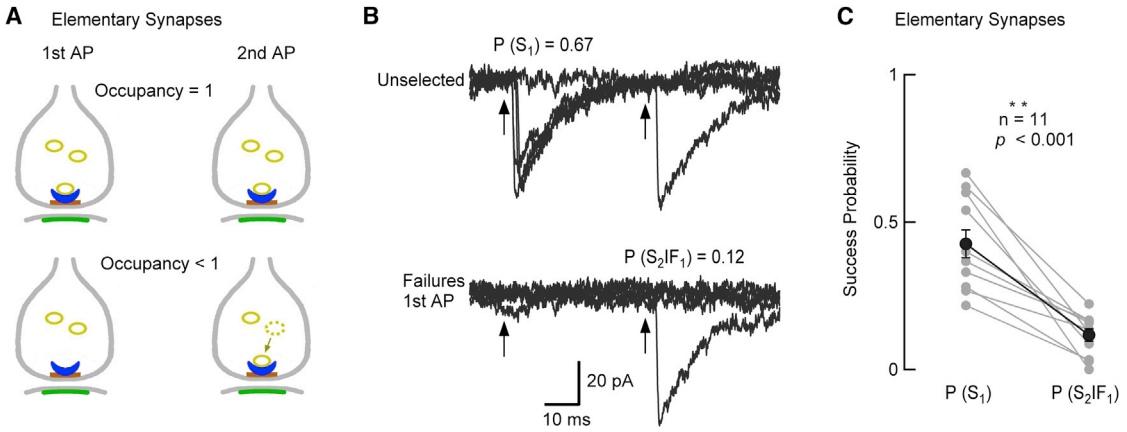

Figure 3. Release Statistics in Elementary Synapses Indicate Incomplete Docking Site Occupancy

(A) Principle of the analysis. In an elementary synapse where the docking site occupancy is 1, failure does not change the status of the synapse; hence, the probability of success for a second AP following a failure, noted $P(S_2IF_1)$, is the same as the original probability of success, noted $P(S_1)$. If on the other hand the docking site occupancy is less than 1, then some failures correspond to occupancy failure, in which case success for a second AP is unlikely because it requires previous refilling of the docking site.

(B) Representative traces from an elementary synapse. Upper panel: Unselected traces, showing a high release probability for the first AP: $P(S_1) = 0.67$. Lower panel: Selected traces showing failures for the first AP. The conditional probability of success for the second AP given that there was a failure for the first one, $P(S_2IF_1)$, is much lower than $P(S_1)$: $P(S_2IF_1) = 0.12$. Presynaptic stimulations marked with arrows.

(C) Summary results from several elementary synapses. In each experiment (gray dots) $P(S_2IF_1)$ is lower than $P(S_1)$. Average values (black dots; mean ± SEM) are, respectively, 0.117 ± 0.021 and 0.426 ± 0.047 ($p < 0.001$; $n = 11$).

2A–2D, respectively, exemplify the cases N = 6 and N = 1. Cells with identical N values cluster together in the plots of Figures 2E and 2F. The mean value of N in these experiments was 2.5, close to the value of 2.0 previously obtained in calcium photolysis experiments (Trigo et al., 2012).

The Resting Occupancy of Docking Sites Is Less than 1

Docking site occupancy at rest is tainted with uncertainty as methods to measure this parameter have been lacking. In view of this information gap, it has often been postulated for simplicity that $\delta = 1$. At the calyx of Held δ is estimated at 0.8 or higher (Neher, 2010). This issue can be addressed by considering simple synapses with N = 1, which we called "elementary synapses" (Figure 2). In these synapses, we examined the conditional probability of success in response to the second pulse given that there is a failure for the first pulse, noted $P(S_2IF_1)$. The rationale to focus on this parameter is as follows. Failures represent either an occupied site that fails to release or an empty site. If $\delta = 1$, all failures belong to the first category. In this case, the site remains occupied after an initial failure, so that the second pulse has still a probability p to elicit release. This is the same probability as that applying for the first pulse (Figure 3A, upper panel). If, however, $\delta < 1$, some of the failures are due to the docking site being empty. Following this class of failure, release is less likely for a second pulse as docking site refilling is slow (Figure 3A, lower panel; see statistical analysis in Experimental Procedures). Therefore if $\delta = 1$, $P(S_1)$ and $P(S_2IF_1)$ should be identical, but if $\delta < 1$, $P(S_2IF_1)$ should be less than $P(S_1)$. Experimental results support the latter possibility. Thus, in the elementary synapse recording of Figure 3B, whereas $P(S_1)$ is 0.67, $P(S_2IF_1)$ is 0.12. In all elementary synapse recordings it was found that $P(S_2IF_1)$ was smaller than $P(S_1)$ (Figure 3C; $p < 0.001$), showing that as a rule, docking site occupancy is less than 1 under resting conditions. (A similar discrepancy is found in experiments with $N > 1$, but the difference is less marked, and the interpretation of the effect is less direct.)

An approximate calculation of p and δ starting from P(S1) and $P(S_2IF_1)$ yields estimates of 0.84 and 0.51, respectively (Experimental Procedures). These values are very compatible with those obtained with more complete calculations as discussed next.

Simulation of Simple Synapse Release Statistics

Once N is determined (starting from $P(S_1)$ and $P(S_2)$, see above), the other model parameters (p, δ, and R) can be calculated as described in Experimental Procedures. The results fail to reveal significant differences linked to the stimulation frequency, which was varied between 25 Hz and 50 Hz (Figure S4). When group results are displayed as a function of N, no significant correlation emerges (Figure S4).

Given the homogeneity of model parameters across experiments (n = 33), a simulation of simple synapse release statistics was performed with a single set of parameters, close to the average values obtained from Figure S4: p = 0.89, δ = 0.45, and R = 3.0 s^{-1}. In each docking site, the mean occupancy decreases with stimulation number, from 0.45 before pulse nb. 1, to 0.164 before pulse nb. 2, 0.136 before pulse nb. 3, and 0.133 before both pulse nb. 4 and pulse nb. 5. Release/failure statistics are then obtained by combining together those of each docking site, depending on the value of N. The simulations predict larger initial success rate, and less depression, for large N values than for small N values (Figure 4A). Although P(S) varies widely across experiments, results of individual experiments are close to the simulation obtained with the relevant N value (Figure 4A).

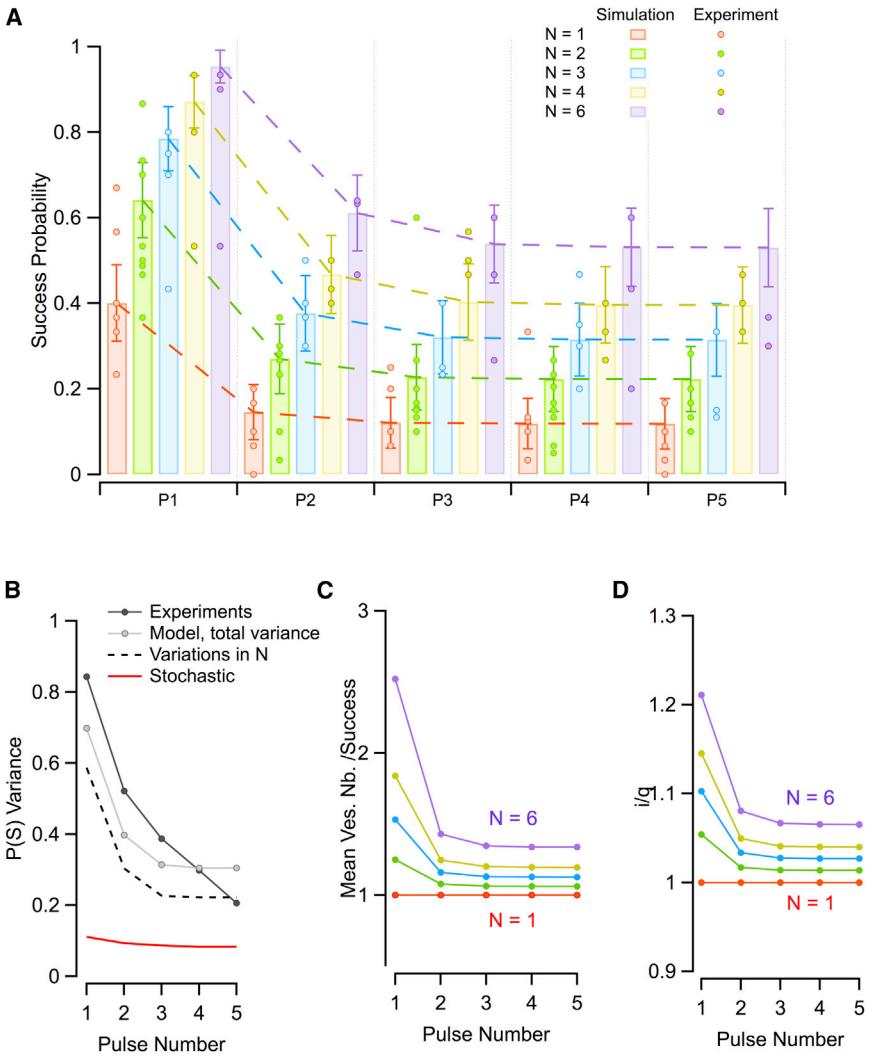

Figure 4. Simulation of Simple Synapse Statistics for Various Docking Site Numbers

(A) Experimental data (circles) and model simulations (bar histograms; error bars represent ± the SD expected from binomial statistics given the data size), depicted P(S) as a function of stimulus number (interstimulus interval: 40 ms). Model parameters are p = 0.89, δ = 0.45, and R = 3 s^{-1}. As N increases from 1 to 6, release probability increases, and synaptic depression decreases.

(B) Comparison between estimated and observed variance of P(S) among experiments. The variance calculated from the simulations of (A) using the pattern of N values experimentally observed (dashed line) was added with the variance expected from the finite size of the data sample (red line, calculated on the basis of binomial statistics) to simulate a series of experiments with no variation in p, δ, or R (gray dots). This total variance was comparable to the observed variance (black dots), indicating little variations of p, δ, or R among synapses.

(C) Simulation of mean number of released vesicles per successful response (see Experimental Procedures). This number varies from 1 for elementary synapses to 2.5 for the first stimulus in N = 6 synapses.

(D) Normalized peak PSC amplitude as a function of pulse number and docking site number. The peak PSC estimated at a simple synapse, i, was normalized by division with the quantal amplitude (q: the peak amplitude reflecting a single vesicular release). This ratio was estimated from the results of (C) assuming a value of 0.76 for the peak receptor occupancy following one vesicular release event (see Experimental Procedures). For elementary synapses the ratio is 1; however, it is larger than 1 for N > 1 synapses because saturation of postsynaptic receptors is incomplete. In the simulation shown, the i/q ratio reaches a maximum of 1.21 for the first pulse response with N = 6.

Figure 4B displays the predicted interexperiment variance of the success probability calculated on the basis of differences in N (dashed black line) and the stochastic variance associated with the finite number of trials that were used in each experiment (red line). The sum of these two components (gray line and dots in Figure 4B) accounts for a large fraction (80% or more) of the observed variance (black line and dots in Figure 4B; n = 33). These results suggest that the primary source of heterogeneity among simple synapses lies in differences in the docking site number. The residual difference between experimental and modeled variances reflects variations in the release parameters p, δ, and R among synaptic sites. These variations appear small, in contrast with the situation found in culture (Ermolyuk et al., 2012).

Variations of PSC Peak Amplitude and Decay Kinetics with Pulse Number

So far we have treated PSCs as a binary process without attempting to disambiguate the number of vesicular release events contributing to each successful response. However, previous work at simple synapses has revealed that responses involving larger numbers of released vesicles have larger peak amplitudes and slower decays than those with smaller vesicle numbers (Kondo and Marty, 1998). This suggests that during a train, mean values for PSC peak amplitude and decay duration should vary with pulse number. Specifically, multivesicular release is predicted to occur mostly for the first pulse, so that the peak amplitude and half time of decay should decrease as a function of pulse number. In addition, these variations should not occur if N = 1, because multivesicular release never happens in this case. Verifying these predictions represents a stringent test of the validity of our experimental and theoretical approaches.

We used the same model as above to describe the mean number of released vesicles per successful trial during a train (Figure 4C). This number decreases within a train following docking site occupancy. However, it also depends on N, with a maximum for the first pulse response near 2.5 in N = 6 synapses and near 1.2 in N = 2 synapses. Starting from these numbers, we simulated the modification of PSC amplitudes during trains. Due to multivesicular release and partial receptor saturation, the peak

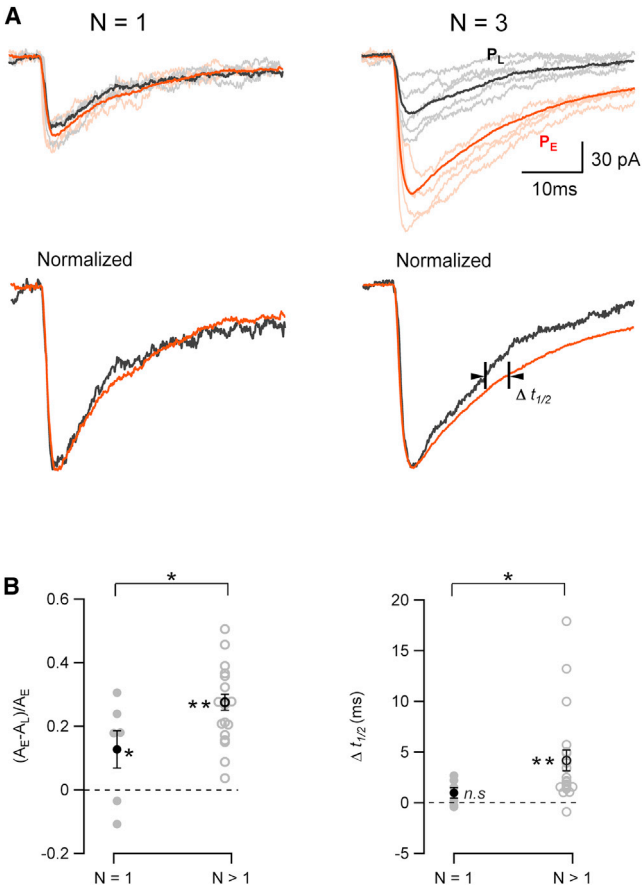

Figure 5. Variations of PSC Peak Amplitude and Decay Kinetics in Simple Synapses

(A) Data from two experiments, one with N = 1 (left) and the other with N = 3 (right). In each experiment, sweeps were selected where one early event was followed by a late event with an interval of ≥80 ms, and early and late events were aligned and superimposed (pink and gray traces respectively). Averages (from 30 trials) were collected for such pairs of early events (labeled P_E, in red) and late events (labeled P_L, in black). Upper panels: Peak amplitudes are larger for P_E than for P_L in the case N = 3 but are similar in the case N = 1. Lower panels: After normalization, decay kinetics appear slower for P_E than for P_L in the case N = 3, but kinetics are very similar in the case N = 1.

(B) Summary data from 11 elementary synapse experiments (N = 1) and 17 additional simple synapse experiments with N > 1. Left: Peak amplitude differences between early and late PSCs as a function of N. In each experiment the mean difference between early and late amplitudes was normalized with respect to the early event amplitude. This difference was significantly larger for N > 1 experiments (gray circles and associated black mean) than for N = 1 data (gray dots and associated black mean; $p < 0.05$). It is interpreted as reflecting an increased degree of receptor activation for the first stimulation following multivesicular release in the N > 1 experiments. Note that N = 1 experiments yield a significant difference in peak amplitudes between early and late PSCs ($p < 0.05$), even though this difference is markedly larger in the case N > 1 (where $p < 10^{-6}$). The origin of this effect is investigated in Figure S4. Right: Half decay time differences between late and early PSCs, as a function of N. Again, a significant difference between early and late events was found in N > 1 experiments (gray circles and black mean: $p < 0.0002$). By contrast, no difference was found in elementary synapses (gray dots and black mean: $p > 0.05$). $\Delta t_{1/2}$ values are significantly larger for N > 1 synapses than for N = 1 synapses ($p < 0.05$). The results indicate that PSC amplitude and decay duration increase with multivesicular release and, furthermore, that multivesicular release decreases as a function of stimulus number for N > 1 experiments, but not in N = 1 experiments.

Error bars represent ± SEM.

PSC amplitude, i, is on average larger than the quantal size q. We calculated the i/q ratio by combining the results of Figure 4C with a previous estimate for the percentage of receptor occupancy at the peak of one quantal event (0.76; Auger et al., 1998). The results predict a maximum i/q ratio of 1.21 for N = 6 and of 1.05 for N = 2 (Figure 4D).

A potential difficulty of this analysis is overlap between successive responses, which could produce nonlinear PSC additivity and obscure some of the expected effects. For this reason, we only analyzed sequences obtained with low stimulation frequency (25 Hz), and we restricted the analysis to sequences that included at least one failure before a late event. In this way, we produced pairs of early and late events separated by at least 80 ms, thus minimizing overlap between paired responses. For experiments where the value of N had been estimated as 1 (elementary synapses, shown in the left column of Figure 5A), amplitude and decay time were similar for early stimulations (red traces) and for late traces (black). By contrast, in N > 1 experiments, early responses displayed larger amplitudes and slower decays than late responses (right column of Figure 5A).

Group results reveal that after normalization with respect to the first event amplitude, the relative difference between early and late PSC amplitudes is significantly larger for N > 1 experiments than for N = 1 experiments (respective mean values: 0.263 ± 0.026, n = 20, and 0.126 ± 0.060, n = 6; $p < 0.05$; Figure 5B, left). Likewise differences in $t_{1/2}$ values between early and late events are significantly larger for N > 1 experiments than for N = 1 experiments (respective mean values: 4.07 ± 1.03 ms, n = 20, and 0.99 ± 0.54 ms, n = 6; $p < 0.01$; Figure 5B, right). These results indicate that both amplitude and kinetic effects are related to a differential mean number of vesicles released per successful event.

An alternative mechanism that could lead to a lengthening of PSC decay is spillover from adjacent synapses (Balakrishnan et al., 2009). While signs of spillover were obtained in a minority of the present recordings (Figure S5), two lines of evidence argue against spillover accounting for $t_{1/2}$ changes during trains. First, spillover does not explain differences in $t_{1/2}$ results between N > 1 and N = 1 synapses, whereas multivesicular release does. Second, it is possible to correct PSC traces for spillover based on the analysis of failures (Figure S5). Results in Figure 5 were corrected in this manner, showing that spillover is insufficient to account for the observed $t_{1/2}$ changes.

Modulation of PSC Amplitude by Receptor Saturation/Desensitization during Trains

Differences between early and late $t_{1/2}$ values, as quoted above, were not significant for elementary synapses ($p > 0.05$), consistent with the notion that no multivesicular release occurs in such cases. Early PSC amplitudes were, however, significantly larger than late PSC amplitudes in elementary synapses ($p < 0.05$). To investigate the origin of this effect we performed GABA uncaging experiments using the fast caged GABA, DPNI-GABA (Trigo

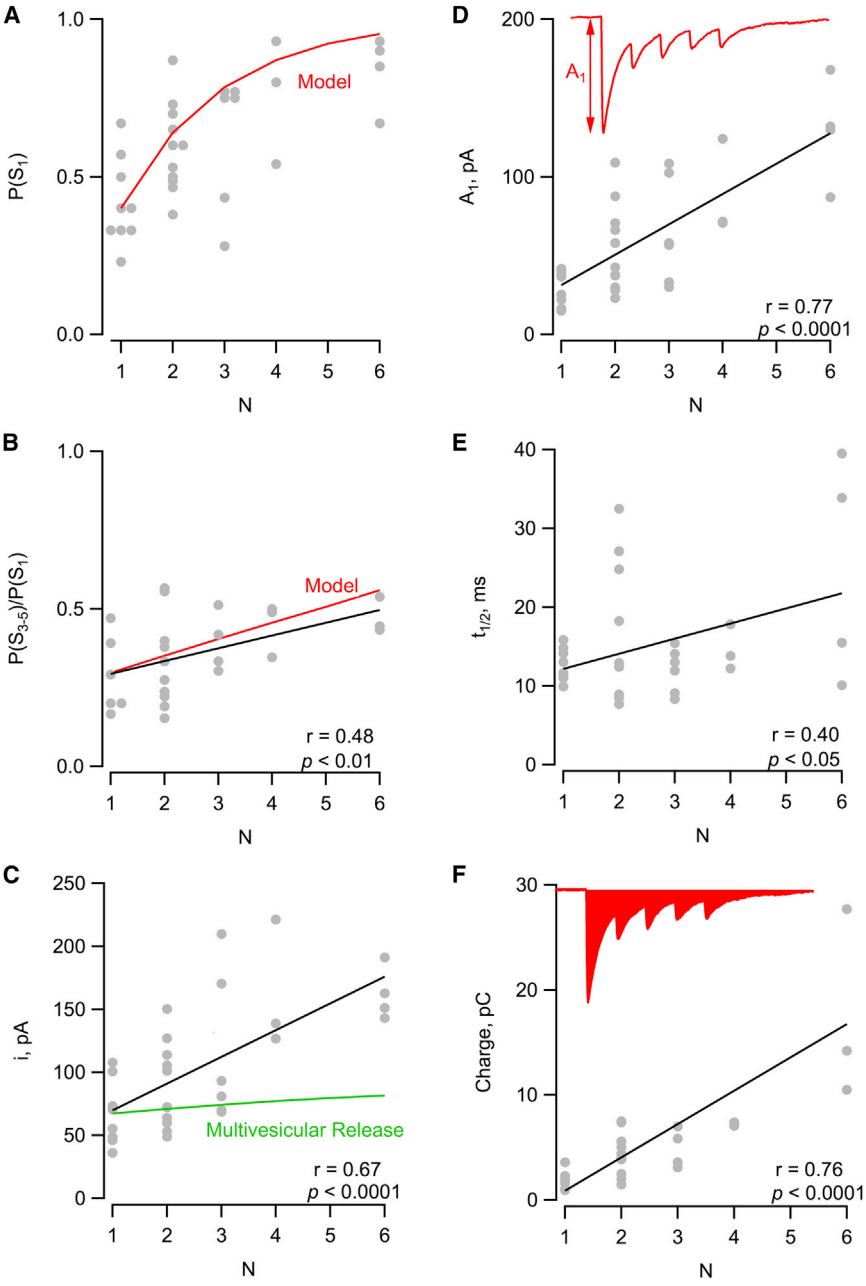

Figure 6. Dependence of Simple Synapse Parameters on Docking Site Number

(A) Dependence of $P(S_1)$ on N (gray circles: experiments; red: model predictions with p = 0.89, δ = 0.45, and R = 3 s^{-1}).

(B) Dependence of $P(S_{3-5})/P(S_1)$ on N (circles: experiments; red: model predictions; black: regression line).

(C) Plot of i as a function of N. The data show a strong positive correlation, suggesting that synapses with small N values are smaller than synapses with large N values (black: regression line). To assess the participation of multivesicular release in the overall dependence of peak PSC amplitude on N, a normalized plot of the predicted i/q ratio as a function of N is shown (green line, from Figure 4D). This curve displays a shallow dependence on N, implying that quantal size, rather than the number of released vesicles, is the major factor underlying variations of i with N.

(D) Mean peak PSC amplitude for the first stimulus (including failures) as a function of N (black: regression line).

(E) Half time of PSC decay (calculated for first responses within a train) as a function of N (black: regression line).

(F) PSC integral during a five-pulse train as a function of N (black: regression line).

et al., 2009). Local uncaging of DPNI-GABA at single varicosities is able to mimic synaptic currents accurately (Trigo et al., 2009). Two consecutive identical stimulations were applied. At intervals of 10 ms, the second stimulation gave a current response that was 56% ± 10% of the first (n = 6), consistent with partial saturation of the receptors (Figure S6A). At intervals of 80 or 100 ms, the second response had recovered much of the initial amplitude, but recovery was incomplete, with a ratio between late and early responses of 0.77 ± 0.05 at 80 ms (n = 10) and 0.81 ± 0.04 at 100 ms (n = 11) (Figure S6B). These results indicate that repeated stimulation at such intervals results in a reduction of the response amplitude by about 20%. This accounts for the residual amplitude effect seen for elementary synapses in Figure 5B.

In conclusion, the results of Figure 5, together with the control experiments of Figures S5 and S6, indicate that multivesicular release shapes PSC amplitudes and decay kinetics during trains and that these effects depend on N values. These results are in agreement with the model of Figure 4 and demonstrate the predictive power of a description of synaptic function based on several docking sites.

Simple Synapse PSCs as a Function of N

Simulations and experimental results describing simple-synapse parameters are presented in Figure 6 where results from each experiment (n = 21–33) are plotted as a function of the N value that is assigned to it. Both simulated (red curve, from the model of Figure 4) and experimental (circles) values of $P(S_1)$ increase steeply between N = 1 and N = 2 and saturate for N values of 3 or higher (Figure 6A). $P(S_{3-5})/P(S_1)$ values grow moderately but significantly as a function of N (Figure 6B; black: regression line, p < 0.01). The model of Figure 4 (red line in Figure 6B) is close to the regression line, showing that variations in docking site numbers account for the paradoxical changes of synaptic depression with synaptic size illustrated in Figure 2F.

In the same way that i is determined by the size of the postsynaptic density, N is likely determined by the size of the active zone. The correspondence between presynaptic and postsynaptic aspects of the synapse therefore suggests that i and N are correlated. When i was plotted as a function of N, a highly significant correlation was indeed revealed ($p < 0.0001$; Figure 6C). This is a remarkable result since the procedure to determine the value of N entirely rests on an analysis of failure patterns and does not consider PSC amplitudes. Equally noteworthy is the size of the effect: the regression line indicates an increase over a 2.4-fold range from N = 1 to N = 6. Because receptor saturation limits the augmentation of PSC amplitude that could result from multivesicular release, this large ratio cannot just reflect increased PSC summation with N (simulation: green curve in Figure 6C). The bulk of the effect of N on i therefore reflects changes in the number of postsynaptic receptors, and consequently of the quantum q, as a function of N.

As N increases, a number of parameters are altered, all contributing to producing an increase in synaptic strength. Since both the probability of success (Figure 6A) and the amplitude of successful events (Figure 6C) increase, the mean peak PSC amplitude (including failures) is expected to increase steeply with N due to a combination of these two effects: this is indeed the case (Figure 6D). The regression line ($p < 0.00001$) indicates an increase in the peak amplitude for the first pulse from 30 pA for N = 1 to 129 pA for N = 6, a ratio of 4.2-fold. Two additional effects contribute to increase synaptic strength during a train. First, the results of Figure 6B indicate that synaptic depression decreases as N increases. Second, the lengthening of PSC decay with multivesicular release (Figure 5) suggests that $t_{1/2}$ may increase as N increases. The examples of Figure 1 (with N = 6, showing slowly decaying PSCs) and Figure 2 (with N = 1, showing faster decaying PSCs) support this possibility. In line with these expectations, when $t_{1/2}$ for the first pulse in a train was plotted as a function of N, a positive correlation was found, indicating that differences in N exert a significant effect on PSC kinetics (Figure 6E; $p < 0.05$; the regression line indicates a 1.8-fold larger $t_{1/2}$ decay value for N = 6 than for N = 1). Finally, to examine the overall effect of N on synaptic transmission, we plotted the synaptic charge corresponding to the integral of the mean PSC elicited by a 25 Hz train, finding a very steep relationship to N (Figure 6F). The regression line ($p < 0.0001$) indicates a mean charge increase from 1.2 pC for N = 1 to 15.5 pC for N = 6, a ratio of 13-fold. Thus, the weight of synaptic signals varies over a very large range for simple synapses, and the value of N stands as the major determinant of this variability.

Changes in Synaptic Properties Induced by Presynaptic Depolarization

The above analysis suggests that the number of docking sites determines intersynaptic variability and that in a given experiment changes in docking sites occupancy account for synaptic depression. We next asked whether it is possible to modulate docking site occupancy by another experimental manipulation.

In MLIs, subthreshold somatic depolarization increases axonal calcium concentration and spontaneous vesicular release (Glitsch and Marty, 1999; Bouhours et al., 2011; Christie et al., 2011). Consequences on subsequent evoked release involve either an increase or no significant change of the release probability and, in both cases, a drop of the paired-pulse ratio (Bouhours et al., 2011; Christie et al., 2011). Here we examined the patterns of success/failures during trains, interleaving tests at the standard holding potential of −60 mV with tests following 9-s-long prepulses at −80 mV or at −50 mV (Figure 7A). In all experiments, presynaptic traces were examined during depolarizing prepulses, and recordings were discontinued if APs were apparent, indicating voltage-clamp escape. We found in agreement to previous data a decrease with depolarizing prepulses for both the PPR (at −80 mV: 0.64 ± 0.08 ; at −60 mV: 0.31 ± 0.08 ; at −50 mV: 0.17 ± 0.04 ; n = 9 ; effects of hyper- and depolarizing prepulses are significant at $p < 0.01$ and $p < 0.05$ levels respectively) and for the ratio $P(S_{3-5})/P(S_1)$ (values normalized with respect to −60 mV data: 1.311 ± 0.152 at −80 mV, $p < 0.05$; 0.737 ± 0.060 at −50 mV, $p < 0.00001$; Figure 7B, lower panel), while the value of $P(S_1)$ did not vary significantly (Figure 7B, upper panel). Assuming that the N value estimated at −60 mV was not modified by prepulses, we compared estimates of p, δ and R obtained at −60 mV with corresponding values with prepulses at −80 mV and at −50 mV. The results revealed a small decrease of p with hyperpolarizing prepulses (with a mean ratio between −80 mV and −60 mV values of 0.955 ± 0.019, $p < 0.02$; Figure 7C, upper panel), no significant change of p with depolarizing prepulses, and no significant change in δ with either hyperpolarizing or depolarizing prepulses (Figure 7C, middle panel). Surprisingly, the recovery rate R was markedly affected by prepulses, particularly in the depolarizing direction, with highly significant variations with respect to control (values normalized to −60 mV data: 1.328 ± 0.121 at −80 mV, $p < 0.01$; 0.710 ± 0.078 at −50 mV, $p < 0.0002$; Figure 7C, lower panel). This indicates that a reduction in R is the major reason for the reduced PPR value and for the decreased release probability found at the end of a train after depolarization. It is well established that an elevation of the presynaptic calcium concentration during trains accelerates vesicular replenishment (Neher and Sakaba, 2008). The present results indicate that an elevation of the calcium concentration prior to a train has the opposite effect, perhaps due to enhanced spontaneous release and to an associated decrease in the content of a reserve pool supplying vesicle replenishment. This mechanism (Figure 7D) is in line with the previous finding that the frequency of spontaneous PSCs increases during depolarizing prepulses (Glitsch and Marty, 1999; Christie et al., 2011), which was confirmed in the present experiments (respective values at −60 mV and −50 mV: 0.299 ± 0.098 and 0.365 ± 0.131 Hz ; $p < 0.001$, n = 5).

Overall, the results suggest that p is modestly sensitive to the prepulse potential, presumably because it is close to saturation, and that R strongly decreases with depolarization, presumably as a consequence of enhanced spontaneous release. It can be shown using Equation 7 below that in the case $p \sim 1$, the late occupancy in a train is proportional to R. Therefore, the change of R alters late release by decreasing docking site occupancy. In summary, the results suggest that docking site occupancy can be specifically modified during synaptic plasticity.

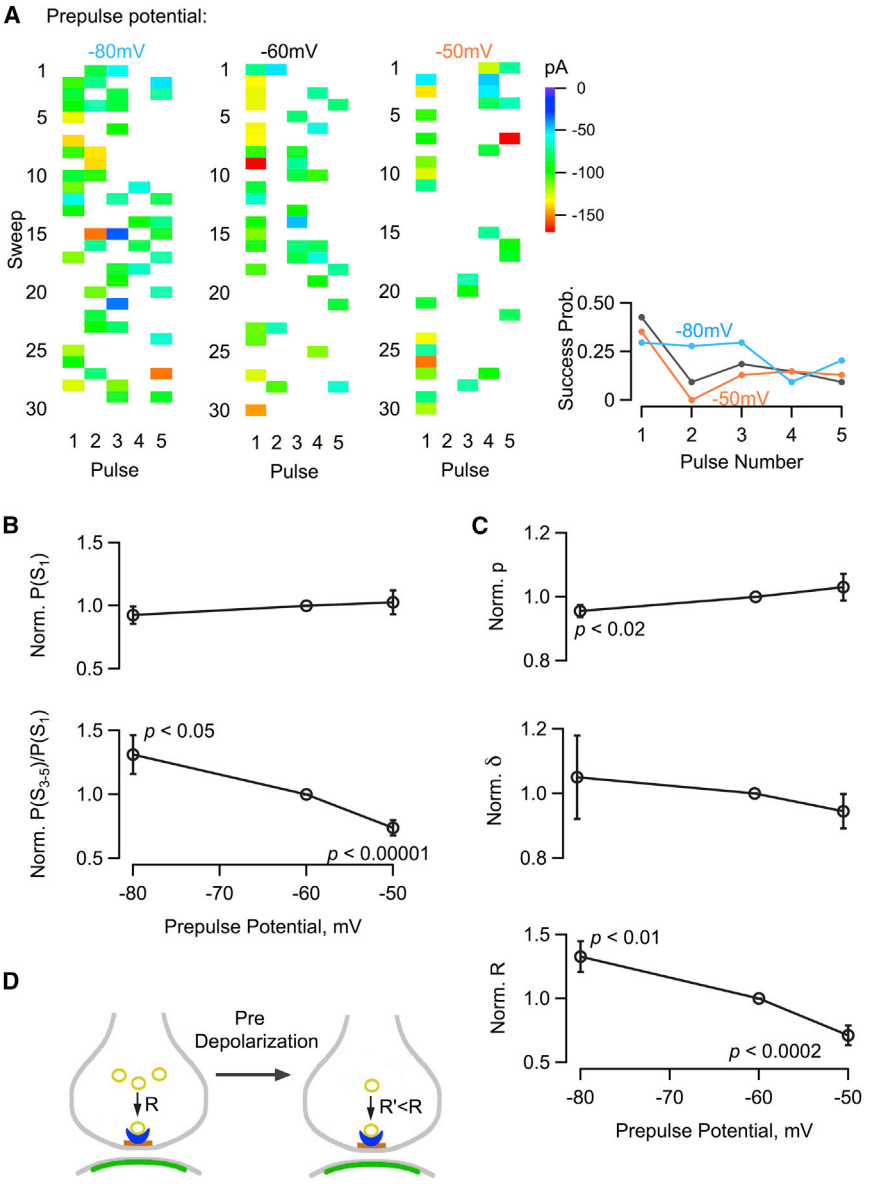

Figure 7. Presynaptic Prepulses Change Vesicular Recruitment Rate

(A) Left: Exemplar experiment showing responses to five-pulse trains delivered from the standard holding potential of −60 mV, preceded by 9-s-long prepulses at −80 mV (left column), at −60 mV (no prepulse; center column), and at −50 mV (right column). The sequence with the three prepulse potentials was repeated as a loop. Right: Plots of $P(S_j)$ for the three potentials, suggesting an increase of synaptic depression with depolarizing prepulses.

(B) Group data (n = 10) showing $P(S_1)$ (upper plot) and $P(S_{3-5})/P(S_1)$ (lower plot) as a function of prepulse potential, after normalization to the value at −60 mV.

(C) Normalized calculated values of single site parameters indicate a small decrease of p with hyperpolarizing prepulses (upper panel), no change of δ (middle panel), and a strong decrease of R with depolarizing prepulses (lower panel).

(D) Model of proposed link between the augmentation of spontaneous synaptic activity during depolarizing prepulses, leading to a depletion of reserve vesicles, and the observed decrease in R during subsequent trains.

Error bars represent ± SEM.

DISCUSSION

A Stochastic Model for Simple Synapses

The present work describes simple synapse function based on a fixed number of docking sites. At each docking site, exocytosis and vesicle replenishment determine occupancy following single-step transitions. Synaptic release statistics are obtained by combining together those of individual docking sites. Multivesicular release, together with postsynaptic receptor saturation, modulate PSC amplitudes and decay kinetics. As explicated in the Experimental Procedures, the model makes a number of assumptions, some of which remain to be tested. Notably, docking sites are supposed to operate independently of each other; rate constants are assumed to be identical among docking sites within a synapse, as well as across synapses. Furthermore, rate constants are assumed to be constant within a train. In spite of its simplicity, the model does capture a number of features of the results, including variations of failure rate and multivesicular release during trains, as well as variations among simple synapses.

Variations in Docking Site Numbers Account for Differences between Simple Synapses

The present work suggests that much of the functional variability observed among simple synapses can be accounted for by variations in a single parameter, the number of docking sites N. Varying N not only accounts for variations of the "presynaptic" parameters, release probability, and paired pulse depression, but also of two major "postsynaptic" parameters: the PSC peak amplitude i and the PSC half decay time $t_{1/2}$. Overall docking site number appears as an integrator of presynaptic and postsynaptic parameters and as a potent organizer of synaptic function.

The relation between i and N uncovered here is very similar to that previously described in the same preparation by Trigo et al. (2012), using a different approach. The close correspondence between the two sets of data would require a highly unlikely coincidence unless the common hypothesis that variable docking site numbers underlie differences among simple synapses is correct. It is well known that the sizes of the active zone and of the postsynaptic density are matched

(e.g., Harris and Stevens, 1988; Schikorski and Stevens, 1997). While previous results indicated that the size of the postsynaptic density determines quantal size (Auger and Marty, 1997; Nusser et al., 1997), the present results, together with those of Trigo et al. (2012), suggest that the size of the active zone determines the number of docking sites. Altogether, larger synapses tend to produce larger signals by a series of complementary effects: larger quantum, larger success probability, larger percentage of receptor activation, slower PSC decay kinetics, and less synaptic depression. While the first effect is linked to the number of postsynaptic receptors, all other effects are the consequence of an increased number of docking sites.

It may be noted that in systems (like GABAergic synapses) where receptors are close to saturation, the range of variation of synaptic efficacy would be limited if synaptic size were fixed. In such systems, increasing synaptic size is a particularly efficient way to increase synaptic strength. However, variations in size, receptor numbers, and quantal amplitude also occur at glutamatergic synapses (Harris and Stevens, 1988; Schikorski and Stevens, 1997; Crowley et al., 2007). It remains to be seen whether this is accompanied with changes in the number of docking sites.

In order to minimize the probability of changes of N within an experiment, we kept presynaptic stimulation sparse, and we restricted the duration of data acquisition to 15 min per cell. While our hypothesis of a fixed N value seems justified under these circumstances, the possibility is clearly open that N may change in response to stronger stimuli, or over longer periods of time, and differences in past synaptic activity may contribute to explaining the differences in N values observed among synapses.

A Special Category of Simple Synapses Exhibits a Single Docking Site

An elementary synapse is a simple synapse that has a single docking site (N = 1; examples in Figures 2 and 3). It never releases more than one vesicle in response to an AP and therefore obeys the ''single-site-single-vesicle'' hypothesis (Korn et al., 1982; Silver et al., 2003). This occurred in 27% of our simple synapses (9/33). Elementary synapses are of special interest since their release statistics are particularly simple. This situation is exploited in the present work to investigate the value of docking site occupancy at rest (Figure 3), but many other applications are possible.

Elementary synapses stand out from other simple synapses (with N > 1) in several ways. They have a lower success probability ($P(S_1)$ = 0.417 ± 0.046 for N = 1 versus 0.662 ± 0.037 for N > 1; n = 9 and n = 24, respectively) and stronger depression ($P(S_{3-5})/P(S_1)$ = 0.285 ± 0.050 for N = 1 versus 0.381 ± 0.028 for N > 1). Their i value (67.7 ± 8.1 pA versus 116.5 ± 10.4 pA; $p < 0.002$) and $t_{1/2}$ values (12.6 ± 0.6 ms versus 16.2 ± 1.8 ms; $p < 0.02$) are clearly smaller. And finally, they display much weaker changes in amplitudes and decay kinetics of PSCs during trains (Figure 5). The finding of this series of distinctive features of elementary synapses confirms the internal consistency of our analysis and validates the procedure used to estimate N.

Comparison with Previous Models

The classical description of PSC statistics at central synapses involves a fixed quantum q, a release probability p_r, and a number of release units N (Zucker et al., 2009). Here we propose a new variant of this model based on three notions that have been envisaged individually before but have only recently been considered in combination (Trigo et al., 2012): (i) postsynaptic receptor saturation, (ii) presence of several independent docking sites in one active zone, and (iii) partial, time-dependent occupancy of the docking sites.

(i) PSC Amplitude and Decay Kinetics Are Modulated by Postsynaptic Receptor Saturation

At simple MLI synapses, responses appear at first sight to vary in an all-or-none manner, but closer inspection reveals that they vary in size and decay kinetics according to the number of release events. Responses to the first stimulus are larger and slower than later responses. The modulation of the peak amplitude follows the predictions of a model where 76% of the receptors are occupied following one release event. Because receptor activation is not complete following one vesicular release event, multivesicular release increases PSC amplitude according to the number of released vesicles.

Even though the decay kinetics of GABAergic PSCs have long been thought to be largely independent of the amplitude and duration of the GABA pulse in the synaptic cleft, the present data confirms and extends previous evidence (Kondo and Marty, 1998) indicating that multivesicular release modulates PSC decay. $GABA_A$ receptors have two agonist binding sites, and both monoliganded and biliganded receptors contribute to the PSC (Jones and Westbrook, 1995). After removal of the agonist, biliganded receptors must shed one GABA molecule to return to the monoliganded state, from where they relax back to the resting state. It takes therefore longer for biliganded receptors than for monoliganded receptors to return to the basal state. While the extent of the effect depends on kinetic rate constants (Jones and Westbrook, 1995), this suggests that multivesicular release slows PSC decay by favoring the recruitment of biliganded receptors over that of monoliganded receptors.

Receptors at central synapses differ widely in their affinity and decay kinetics. At most GABAergic synapses, vesicular release induces significant receptor occupancy, albeit to different degrees (Auger and Marty, 1997; Nusser et al., 1997; Perrais and Ropert, 1999; Kirischuk et al., 2002; Biró et al., 2006). There is also evidence for a significant degree of receptor occupancy at various types of glutamatergic synapes (climbing fiber synapses onto Purkinje cells: Foster et al., 2002; calyx of Held: Scheuss et al., 2002; parallel fiber input to MLIs: Crowley et al., 2007). Thus, our findings are potentially relevant to both excitatory and inhibitory synapses.

(ii) Within One Simple Synapse, Binomial N Reflects the Number of Docking Sites

The proposal that exocytosis occurs at individual release units can be traced back to Katz (1969), but the nature and very existence of these release units has remained controversial ever since. The strongest functional evidence in favor of release units in central synapses is the fact that fluctuations in synaptic current peak amplitudes decrease at high calcium concentration,

which suggests that the underlying release statistics are binomial rather than Poissonian (e.g., Silver et al., 2003; reviewed in Zucker et al., 2009; Neher, 2010). Previous interpretations of the morphological representation of the number N of release units have varied. According to the single-site-single-vesicle hypothesis, N represents the number of presynaptic varicosities (Korn et al., 1982; Silver et al., 2003). Quantitative studies at the calyx of Held suggest, however, that the number of release competent vesicles is six per active zone and that, therefore, N must be larger than the number of active zones (Neher and Sakaba, 2008). In addition, evidence for multivesicular release has been accumulating at other central glutamatergic (Wadiche and Jahr, 2001; Christie and Jahr, 2006; Crowley et al., 2007) and GABAergic synapses (Biró et al., 2006). These results are difficult to reconcile with the single-site-single-vesicle hypothesis, but they are consistent with the present proposal that N represents the number of docking sites and that several docking sites operate in parallel in one active zone.

(iii) Evidence for Partial Docking Site Occupancy at Rest

Our previous work using calcium uncaging suggested that occupancy of docking sites at rest is less than 1 (Trigo et al., 2012). Two lines of evidence of the present work indicate the same. One is derived from our examination of the conditional probability of release following a failure in elementary synapses (Figure 3). The result that δ is less than 1 can alternatively be derived from modeling the mean frequencies of failures according to the estimated number of docking sites (Figure 4). This finding implies that, at rest, the reaction leading to docking site occupancy is reversible by a mechanism that remains to be elucidated (e.g., reversal of vesicle docking, spontaneous exocytosis, or steric hindrance between docked vesicles). It also implies that the RRP at rest is not fixed. Altogether, synaptic release results from a combination of two stochastic processes, and not of a single process, as commonly assumed: docking site occupancy with probability δ and exocytosis with probability p.

Docking Site Occupancy and Replenishment Rate as Potential Targets of Synaptic Plasticity

The standard description of simple synapses focuses on a single adjustable presynaptic parameter, the release probability p_r (Zucker et al., 2009). In contrast, the present description contains three presynaptic parameters (p, δ, and R), raising the possibility that each of these parameters could be adjusted as a function of specific forms of neuronal activity. The initial release probability is given by a combination of p and δ, whereas late release depends on a combination of p and R. Our results show that applying presynaptic prepulses results in variations of R, leading to changes in docking site occupancy and release probability during the late phase of a train (Figure 7). This demonstrates that docking site replenishment can be modified by previous neuronal activity. It will be interesting in future work to investigate whether manipulations leading to changes in p_r target p, δ, or both. In general, the present description of single site function offers an opportunity to characterize synaptic plasticity in a more specific manner than in previous treatments, thus opening a new path toward underlying cellular mechanisms.

EXPERIMENTAL PROCEDURES

Electrophysiological Recordings

Cerebellar slices were prepared from rats aged PN 12–14. All experiments were performed at room temperature. Recording procedures are detailed in Supplemental Information.

Binomial Model of Simple Synapses

We consider a simple synapse containing N equivalent docking sites. Each docking site has an initial probability δ of being occupied by a release-ready vesicle. An occupied docking site has a probability p to undergo exocytosis, which is assumed to remain constant throughout the train. After exocytosis, the emptied docking site has a probability r to become release competent during one interpulse interval Δt. Assuming a recovery reaction with a single rate constant R, the link between r and R is $r = 1 - e^{-R\Delta t}$. We suppose for simplicity that docking sites are independent of each other and that δ, p, and r are identical across docking sites.

Under the above assumptions, the probability of one docking site to release in response to the j^{th} stimulation is

$$P_D(S_j) = \delta_j p, \tag{3}$$

where δ_j is the docking site occupancy before pulse number j. For j = 1, we note $\delta_1 = \delta$.

Because all sites are independent, the probability of having simultaneously a failure at all N sites is

$$P(F_j) = (1 - P_D(S_j))^N = (1 - \delta_j p)^N. \tag{4}$$

Hence, the probability to have at least one vesicular release event in response to pulse number j is

$$P(S_j) = 1 - (1 - \delta_j p)^N. \tag{5}$$

This model can be considered as a probabilistic variant of the previous macroscopic model by Tsodyks and Markram (1997). It assumes that two nested stochastic processes contribute to release statistics, whereas the traditional synaptic model (Equation 9, below) considers a single stochastic process. Here the evolution of $P(S_j)$ during a train is governed by δ_j. For each docking site, the probability of occupancy before pulse (j + 1), δ_{j+1}, is the sum of the probability that an occupied site at pulse j fails to release at pulse j, plus the probability that an occupied site at pulse j releases at pulse j and recovers between pulse j and pulse (j + 1), plus the probability that an unoccupied site at pulse j recovers between pulse j and pulse (j + 1):

$$\delta_{j+1} = \delta_j(1 - p) + \delta_j p r + (1 - \delta_j) r. \tag{6}$$

We note that this equation predicts depression if $\delta > r/(r + p(1 - r))$, but that it predicts facilitation if $\delta < r/(r + p(1 - r))$. The first inequality applies for any set of (r, p) values if δ = 1, because the ratio $r/(r + p(1 - r))$ is less than 1. In general, high values of δ and/or p favor depression, and high values of r favor facilitation. At steady state, $P(S_j)$ reaches a value L, which is independent of j. By entering $P(S_j) = L$ and $\delta_{j+1} = \delta_j$ in Equations 5 and 6, one obtains

$$r = \frac{p\lambda}{p\lambda + p - \lambda}, \tag{7}$$

where $\lambda = 1 - (1 - L)^{1/N}$.

If N is known, Equations 5, 6, and 7 can be used to calculate the unknowns (p, r, and δ) from the measurable parameters $P(S_1)$, $P(S_2)$, and L. The solution for p reads

$$p = \frac{\lambda + 1 + ((\lambda + 1)^2 - 4\lambda B)^{1/2}}{2B} \tag{8}$$

with $B = 1 - P(F_1)^{\frac{1}{N}} - \lambda \Big/ 1 - P(F_2)^{\frac{1}{N}} - \lambda$.

Having calculated p from Equation 8, r can be calculated from Equation 7 and finally δ from Equation 5 with j = 1.

Estimating N

To obtain a first estimate for N, we make two simplifying assumptions. First, we assume that the RRP size applying before the first pulse is fixed in one given experiment, with a value n = δN. Second, we neglect the recovery rate by making r = 0. In view of the first assumption, the failure probability after the first pulse takes the previously used form (e.g., Dobrunz and Stevens, 1997; Hanse and Gustafsson, 2001):

$$P(F_1) = (1-p)^n. \quad (9)$$

This equation follows the predictions of a binomial process with δN units having each a release probability p, whereas in the previous version of the model, we had a binomial process with N units having each a release probability δp. After the first pulse the RRP size drops from the initial value n to the new value $n(1-p)$. Under the assumption that r = 0, and assuming again that the RRP size does not fluctuate around its mean value, we have

$$P(F_2) = (1-p)^{n(1-p)}. \quad (10)$$

These two equations can be combined to yield

$$n = \frac{log(1-P(S_1))}{log(log(1-P(S_2))/log(1-P(S_1)))}. \quad (11)$$

Values obtained with Equation (11) ranged between 0 and 3. To obtain N, we assumed that the occupancy δ was close to the value 0.7 previously obtained (Trigo et al., 2012). Therefore, N was initially chosen as the integer closest to the ratio n/0.7. Once complete, p, δ, and R calculations were made according to Equations 5, 6, 7, and 8, new N values were estimated due to the fact that the calculated δ value was different from the initial value of 0.7 and, if needed, a new set of calculations was performed in an iterative manner until the value of N became stable. In addition, when the procedure returned the result N = 1, indicating an elementary synapse, individual responses were examined to identify potential double vesicular release events. When such responses were found, the experiment was reclassified as N = 2 (3 such reclassifications out of 14 experiments that were initially classified as N = 1).

For some experiments the calculation led to an apparent value of p that was >1. Such values were not accepted. Instead, a value p = 1 was introduced, and values of δ and R were recalculated according to Equations 5 and 7.

Elementary Synapse Statistics

For elementary synapses N = 1.

In this case, Equation 5 applied to the first pulse (j = 1) simplifies to

$$P(S_1) = \delta p. \quad (12)$$

The conditional probability to observe a success in response to the second pulse given that a failure was obtained in response to the first pulse is

$$P(S_2|F_1) = \frac{(1-\delta)rp + \delta(1-p)p}{1-\delta p}. \quad (13)$$

Equation 13 indicates that a sequence of failure for the first pulse followed by success for the second pulse can reflect an unoccupied docking site being replenished between the two pulses, and then releasing at the second stimulus, or alternatively an occupied site not releasing during the first stimulus, and releasing during the second one. To understand the implications of this equation it is useful to consider the simplified case where recovery is neglected (R = r = 0). Equation 13 then simplifies to

$$P(S_2|F_1) = \frac{\delta p(1-p)}{1-\delta p}. \quad (14)$$

By combining with Equation 12, this can be rewritten

$$\frac{P(S_2|F_1)}{P(S_1)} = \frac{(1-p)}{1-\delta p}. \quad (15)$$

This ratio is smaller than 1 except for the case $\delta = 1$, where it takes the value of 1.

Solving Equations 12 and 15 given the experimental values $P(S_1) = 0.426$ and $P(S_2|F_1) = 0.117$ gives p = 0.84 and δ = 0.51.

SUPPLEMENTAL INFORMATION

Supplemental Information includes six figures and Supplemental Experimental Procedures and can be found with this article online at http://dx.doi.org/10.1016/j.neuron.2014.12.006.

ACKNOWLEDGMENTS

This work was supported by a Paris Descartes University PhD fellowship to C.P., a combined CNRS/ Paris Descartes Excellence Chair to F.F.T., and an ERC Advanced grant ("SingleSite") to A.M. We thank Philippe Ascher, Guadalupe Astorga, Jin Bao, David Ogden, and Brandon Stell for comments on the manuscript.

Accepted: November 26, 2014
Published: December 24, 2014

REFERENCES

Auger, C., and Marty, A. (1997). Heterogeneity of functional synaptic parameters among single release sites. Neuron *19*, 139–150.

Auger, C., Kondo, S., and Marty, A. (1998). Multivesicular release at single functional synaptic sites in cerebellar stellate and basket cells. J. Neurosci. *18*, 4532–4547.

Balakrishnan, V., Kuo, S.P., Roberts, P.D., and Trussell, L.O. (2009). Slow glycinergic transmission mediated by transmitter pooling. Nat. Neurosci. *12*, 286–294.

Biró, A.A., Holderith, N.B., and Nusser, Z. (2006). Release probability-dependent scaling of the postsynaptic responses at single hippocampal GABAergic synapses. J. Neurosci. *26*, 12487–12496.

Bouhours, B., Trigo, F.F., and Marty, A. (2011). Somatic depolarization enhances GABA release in cerebellar interneurons via a calcium/protein kinase C pathway. J. Neurosci. *31*, 5804–5815.

Branco, T., and Staras, K. (2009). The probability of neurotransmitter release: variability and feedback control at single synapses. Nat. Rev. Neurosci. *10*, 373–383.

Christie, J.M., and Jahr, C.E. (2006). Multivesicular release at Schaffer collateral-CA1 hippocampal synapses. J. Neurosci. *26*, 210–216.

Christie, J.M., Chiu, D.N., and Jahr, C.E. (2011). $Ca^{(2+)}$-dependent enhancement of release by subthreshold somatic depolarization. Nat. Neurosci. *14*, 62–68.

Crowley, J.J., Carter, A.G., and Regehr, W.G. (2007). Fast vesicle replenishment and rapid recovery from desensitization at a single synaptic release site. J. Neurosci. *27*, 5448–5460.

Dobrunz, L.E., and Stevens, C.F. (1997). Heterogeneity of release probability, facilitation, and depletion at central synapses. Neuron *18*, 995–1008.

Ermolyuk, Y.S., Alder, F.G., Henneberger, C., Rusakov, D.A., Kullmann, D.M., and Volynski, K.E. (2012). Independent regulation of basal neurotransmitter release efficacy by variable Ca^2+ influx and bouton size at small central synapses. PLoS Biol. *10*, e1001396.

Foster, K.A., Kreitzer, A.C., and Regehr, W.G. (2002). Interaction of postsynaptic receptor saturation with presynaptic mechanisms produces a reliable synapse. Neuron *36*, 1115–1126.

Glitsch, M., and Marty, A. (1999). Presynaptic effects of NMDA in cerebellar Purkinje cells and interneurons. J. Neurosci. *19*, 511–519.

Hanse, E., and Gustafsson, B. (2001). Paired-pulse plasticity at the single release site level: an experimental and computational study. J. Neurosci. *21*, 8362–8369.

Harris, K.M., and Stevens, J.K. (1988). Dendritic spines of rat cerebellar Purkinje cells: serial electron microscopy with reference to their biophysical characteristics. J. Neurosci. *8*, 4455–4469.

Holderith, N., Lorincz, A., Katona, G., Rózsa, B., Kulik, A., Watanabe, M., and Nusser, Z. (2012). Release probability of hippocampal glutamatergic terminals scales with the size of the active zone. Nat. Neurosci. *15*, 988–997.

Jones, M.V., and Westbrook, G.L. (1995). Desensitized states prolong $GABA_A$ channel responses to brief agonist pulses. Neuron *15*, 181–191.

Katz, B. (1969). The release of transmitter substances (The Sherrington Lectures X). (Springfield: Charles C. Thomas Publisher).

Kirischuk, S., Clements, J.D., and Grantyn, R. (2002). Presynaptic and postsynaptic mechanisms underlie paired pulse depression at single GABAergic boutons in rat collicular cultures. J. Physiol. *543*, 99–116.

Kondo, S., and Marty, A. (1998). Synaptic currents at individual connections among stellate cells in rat cerebellar slices. J. Physiol. *509*, 221–232.

Korn, H., Mallet, A., Triller, A., and Faber, D.S. (1982). Transmission at a central inhibitory synapse. II. Quantal description of release, with a physical correlate for binomial n. J. Neurophysiol. *48*, 679–707.

Llano, I., and Gerschenfeld, H.M. (1993). Inhibitory synaptic currents in stellate cells of rat cerebellar slices. J. Physiol. *468*, 177–200.

Nagwaney, S., Harlow, M.L., Jung, J.H., Szule, J.A., Ress, D., Xu, J., Marshall, R.M., and McMahan, U.J. (2009). Macromolecular connections of active zone material to docked synaptic vesicles and presynaptic membrane at neuromuscular junctions of mouse. J. Comp. Neurol. *513*, 457–468.

Neher, E. (2010). What is rate-limiting during sustained synaptic activity: vesicle supply or the availability of release sites. Front. Synaptic. Neurosci. *2*, 144.

Neher, E., and Sakaba, T. (2008). Multiple roles of calcium ions in the regulation of neurotransmitter release. Neuron *59*, 861–872.

Nusser, Z., Cull-Candy, S., and Farrant, M. (1997). Differences in synaptic GABA(A) receptor number underlie variation in GABA mini amplitude. Neuron *19*, 697–709.

Perrais, D., and Ropert, N. (1999). Effect of zolpidem on miniature IPSCs and occupancy of postsynaptic GABAA receptors in central synapses. J. Neurosci. *19*, 578–588.

Pouzat, C., and Marty, A. (1998). Autaptic inhibitory currents recorded from interneurones in rat cerebellar slices. J. Physiol. *509*, 777–783.

Pouzat, C., and Marty, A. (1999). Somatic recording of GABAergic autoreceptor current in cerebellar stellate and basket cells. J. Neurosci. *19*, 1675–1690.

Sakaba, T. (2008). Two Ca(2+)-dependent steps controlling synaptic vesicle fusion and replenishment at the cerebellar basket cell terminal. Neuron *57*, 406–419.

Scheuss, V., Schneggenburger, R., and Neher, E. (2002). Separation of presynaptic and postsynaptic contributions to depression by covariance analysis of successive EPSCs at the calyx of held synapse. J. Neurosci. *22*, 728–739.

Schikorski, T., and Stevens, C.F. (1997). Quantitative ultrastructural analysis of hippocampal excitatory synapses. J. Neurosci. *17*, 5858–5867.

Sheng, J., He, L., Zheng, H., Xue, L., Luo, F., Shin, W., Sun, T., Kuner, T., Yue, D.T., and Wu, L.-G. (2012). Calcium-channel number critically influences synaptic strength and plasticity at the active zone. Nat. Neurosci. *15*, 998–1006.

Silver, R.A., Lubke, J., Sakmann, B., and Feldmeyer, D. (2003). High-probability uniquantal transmission at excitatory synapses in barrel cortex. Science *302*, 1981–1984.

Szule, J.A., Harlow, M.L., Jung, J.H., De-Miguel, F.F., Marshall, R.M., and McMahan, U.J. (2012). Regulation of synaptic vesicle docking by different classes of macromolecules in active zone material. PLoS ONE *7*, e33333.

Trigo, F.F., Papageorgiou, G., Corrie, J.E.T., and Ogden, D. (2009). Laser photolysis of DPNI-GABA, a tool for investigating the properties and distribution of GABA receptors and for silencing neurons *in situ*. J. Neurosci. Methods *181*, 159–169.

Trigo, F.F., Sakaba, T., Ogden, D., and Marty, A. (2012). Readily releasable pool of synaptic vesicles measured at single synaptic contacts. Proc. Natl. Acad. Sci. USA *109*, 18138–18143.

Tsodyks, M.V., and Markram, H. (1997). The neural code between neocortical pyramidal neurons depends on neurotransmitter release probability. Proc. Natl. Acad. Sci. USA *94*, 719–723.

Wadiche, J.I., and Jahr, C.E. (2001). Multivesicular release at climbing fiber-Purkinje cell synapses. Neuron *32*, 301–313.

Xu, J., and Wu, L.-G. (2005). The decrease in the presynaptic calcium current is a major cause of short-term depression at a calyx-type synapse. Neuron *46*, 633–645.

Zucker, R.S., Kullmann, D.M., and Schwarz, T.L. (2009). Release of neurotransmitters. In From Molecules to Networks, J.H. Byrne and J.L. Roberts, eds. (Waltham: Academic Press), pp. 217–266.